IEEE Access
Multidisciplinary | Rapid Review | Open Access Journal

Received November 23, 2018, accepted December 13, 2018, date of publication December 20, 2018,
date of current version January 11, 2019.

Digital Object Identifier 10.1109/ACCESS.2018.2888540

QFM Signals Parameters Estimation Based on Double Scale Two Dimensional Frequency Distribution

FULONG JING, CHUNJIE ZHANG, WEIJIAN SI, YU WANG, AND SHUHONG JIAO
College of Information and Communication Engineering, Harbin Engineering University, Harbin 150001, China

Corresponding author: Chunjie Zhang (zhangchunjie@hrbeu.edu.cn)

This work was supported in part by the National Natural Science Foundation of China under Grant 61671168 and Grant 61801143, in part by the Fundamental Research Funds for the Central Universities under Grant HEUCF180801 and Grant HEUCFJ180801, and in part by the Natural Science Foundation of Heilongjiang Province of China under Grant QC2016085.

ABSTRACT This paper proposes a novel estimation method, named double scale two dimensional frequency distribution (DSTFD), to estimate the parameters of quadratic frequency modulated (QFM) signals. In the DSTFD, by using a novel parametric instantaneous self-correlation function and the idea of the keystone transform, the QFM signals are transformed into two-dimensional frequency domain, and the QFM signals are detected by searching peaks. To reduce computational cost, a double scale (DS) estimation strategy, which consists of coarse estimation and fine estimation, is proposed. The DS estimation strategy can be implemented by using the Chirp Z-transform and an improved transform named local scaled Fourier transform (LSFT). The LSFT only consists of complex multiplications, fast Fourier transform (FFT), and inverse FFT operations. The implementation, anti-noise performance, and computational cost are analyzed for the proposed method. Through simulations and analyses, the results demonstrate that the DSTFD outperforms other compared algorithms.

INDEX TERMS Double scale two dimensional frequency distribution (DSTFD), quadratic frequency modulated (QFM), parameter estimation, parametric instantaneous self-correlation function (PISCF), double scale estimation strategy.

I. INTRODUCTION

Quadratic Frequency Modulated (QFM) signals are widely used in many fields such as radar, sonar, and communication [1]–[4]. In recent years, parameters estimation and detection of the QFM signals whose frequencies vary quickly with time have received considerable attention, such as the low probability interception radar signal [1].

Maximum likelihood (ML) based methods [5]–[7] are the famous estimation method because of their good anti-noise performance, but they need to search the maximum in the three dimensional domain which leads to a large amount of computation. To reduce the computational cost, many improved methods are proposed. For example, the methods similar to time-frequency analysis technique are proposed, which include the L-class of fourth-order complex-lag PWVD [8], local polynomial Wigner distribution [9], [10], quasi-maximum-likelihood (QML) [11], and the method based on sparsity exploitation [12]. These algorithms have problems of the low anti-noise performance and serious cross-term interference. In addition to the time-frequency methods, some correlation algorithms are proposed. The cubic phase function (CPF) [1], [13] and Higher order ambiguity function (HAF) [14] are the popular correlation estimation methods, whose essence are to reduce the order of QFM signal by the multilinear and bilinear transforms and estimate the parameters by dechirping. Although the computational cost is reduced, the cross-term problem is appeared. In order to eliminate the cross-terms, two categories are exploited: one category is based on product and integrating, and other one is based on two-dimensional parametric domain. The first category methods mainly include the integrated generalized ambiguity function (IGAF) [15], the product HAF (PHAF) [16], the product generalized CPF (PCPF) [17], the product high-order matched-phase transform (PHMT) [18], and the HAF-integrated CPF (HAF-ICPF) [19], where the performance of HAF-ICPF outperforms that of the other methods. The second category methods mainly include the chirp rate and the quadratic chirp rate distribution (CRQCRD) [20], the modified CRQCRD (mCRQCRD) [21], the two-dimensional

product modified parameterized chirp rate-quadratic chirp rate distribution (2D-PMPCRD) [22], the scaled Fourier transform (SCFT) based algorithm [23], the scaled double-autocorrelation transform (SCDCT) [24], and the algorithm presented in [25]. For the CRQCRD, mCRQCRD, and the 2D-PMPCRD, the non-uniform fast Fourier transform (NUFFT) is used to eliminate the brute-force searching. As the NUFFT needs to perform interpolation operation, it is non-preferred in realistic applications. Compared to them, the SCFT based algorithm, the SCDCT algorithm, and the algorithm presented in [25] obtain better estimation performance by using the fast Fourier transform (FFT) instead of the NUFFT, where the performance of the algorithm presented in [25] is better than that of the other two algorithms. Compared to the ML-based methods, although the computational costs of the correlation algorithms are lower, the anti-noise performance and suppression cross-term performance are worse which need to be improved.

Through comprehensive analysis, the algorithm presented in [25] and the HAF-ICPF are selected as the compared algorithms. However, the anti-noise performance of them is still low, and the computational costs are large for high precision estimating. To solve these problems, in this paper, a novel self-correlation algorithm named double scale two-dimension frequency domain (DSTFD) is proposed. By employing a novel parametric instantaneous self-correlation function (PISCF) and the idea of keystone transform operations, the anti-noise performance is improved. In the proposed algorithm, a double scale (DS) estimation strategy is proposed which can reduce the amount of calculation effectively. The DS strategy is implemented by using an improved transform named local scaled Fourier transform (LSFT) and Chirp Z-transform (CZT), where the LSFT only consists of complex multiplications, IFFT and FFT operations. Through the analyses of implementation, anti-noise ability, and computational cost, the DSLVD outperforms the compared algorithms.

The rest of the paper is organized as follows. In Section II, some related works about the proposed method are introduced. In Section III, the proposed method is described. Section IV demonstrates the effectiveness of the DSTFD with a few numerical experiments. Finally, Section V concludes the paper and presents the future research direction.

II. RELATED WORK

In this Section, the key technologies of the proposed algorithm are described, including the PISCF and peak accumulation.

A. THE PISCF

Consider a noise-free multi-component QFM signals which can be described by

$$\begin{aligned} s_m(t) &= \sum_{i=1}^{K} A_i \exp\left(j\phi_i(t)\right) \\ &= \sum_{i=1}^{K} A_i \exp\left(j2\pi\left(a_{1i}t + a_{2i}t^2 + a_{3i}t^3\right)\right) \end{aligned} \tag{1}$$

where K denotes the number of components, $\phi_i(t)$ denotes the signal phase of the ith component, A_i denotes amplitude, a_{1i}, a_{2i}, and a_{3i} are the phase coefficients.

The corresponding instantaneous frequency rate (IFR) of (1) can be represented as

$$\mathrm{IFR} = \frac{d^2\phi_i(t)}{dt^2} = 4\pi\left(a_{2i} + 3a_{3i}t\right) \tag{2}$$

Based on the format of the IFR and the analyses in [20], [26], and [27], a novel parametric instantaneous self-correlation function (PISCF) is defined as

$$\begin{aligned} R_{s_m}(t,\tau) = s_m\left(t + \frac{\tau + a}{2}\right) s_m\left(t - \frac{\tau + b}{2}\right) \\ \times s_m^*\left(t - \frac{\tau + a}{2}\right) s_m^*\left(t + \frac{\tau + c}{2}\right) \end{aligned} \tag{3}$$

where $*$ and τ denote the complex conjugation and the lag time variable, respectively. a, b, and c are constant delay which are utilized to complete order reduction and energy accumulation [27], where $b = a + 2\varpi$ and $c = a - 2\varpi$. ϖ is an order reduction factor described in [16], [27], and [28] whose purpose is to reduce the signal order. According to the analysis in [28] and [30], by using the constant delay a and ϖ, the anti-noise performance is improved. Moreover, the delay a helps to avoid the non-uniformly spaced lag-time axis which is beneficial to improve estimation accuracy [26], [27]. The selection criterions of a and ϖ will be introduced in Section III-C.

Substituting (1) into (3) yields

$$\begin{aligned} &R_{s_m}(t,\tau) \\ &= \sum_{i=1}^{K} A_i^4 \exp\Big[j2\pi\Big((2a_{2i}\varpi - 3a_{3i}\varpi^2)(a+\tau) \\ &\quad + 6a_{3i}\varpi(a+\tau)t\Big)\Big] + R_{cross}(t,\tau) \end{aligned} \tag{4}$$

where $R_{cross}(t,\tau)$ denotes the cross-term. It is easily seen from (4) that the time variable t and lag variable τ couple with each other. Due to the existence of coupling, the phase coefficients are difficult to be estimated.

B. PEAK ACCUMULATION

According to the analysis in [26], the similar coupling can be removed by using the keystone transformation. To remove the coupling in (4), we are inspired by the idea of keystone transformation and propose an improved transformation operation which consists of the local scaled Fourier transform (LSFT) and the inverse Fourier transform (IFT), and the operation is defined by

$$\begin{aligned} x(t_{new}) &= \mathrm{IFT}_f\left[\mathrm{LSFT}_t[x(t)]\right] \\ &= \mathrm{IFT}_f\left[b\int x(t)\exp\left(-j2\pi bft\right)dt\right] \end{aligned} \tag{5}$$

where $t_{new} = t/b$, b is a scaling factor whose purpose is to change the time variable. $\mathrm{IFT}_f[\cdot]$ denotes the IFT operation with respect to f. f is the searching frequency which is limited

in the frequency range $[f_d, f_u]$. f_u and f_d are the upper limit and lower limit of the searching frequency, respectively, which are determined by the frequency range of $x(t)$. When the frequency range of $x(t)$ is unknown in advance, the f_u and f_d are set to the limiting values (without violating Nyquist frequency constraints), which means that $f_d = -f_s/2$ and $f_u = f_s/2$ where f_s is sampling frequency. When the range is known in advance, f_u and f_d are set to the known values. In this paper, the frequency range is unknown.

It is easily seen from (5) that, after performing the LSFT-IFT operation, time variable is changed from t to t_{new}. According to the property of (5), setting $b = \frac{1}{(a+\tau)q}$ and replacing $x(t)$ by $R_{s_m}(t,\tau)$ yield

$$\begin{aligned} R_{s_m}(t_{new},\tau) &= mathrmIFT_f[\mathrm{LSFT_t}\left(R_{s_m}(t,\tau)\right)] \\ &= \sum_{i=1}^{K} A_i^4 \exp\left(j2\pi\left(h_{1i}(a+\tau)+h_{2i}t_{new}\right)\right) \\ &\quad + \mathrm{IFT}_f[\mathrm{LSFT}_t\left(R_{cross}(t,\tau)\right)] \end{aligned} \tag{6}$$

where $t_{new} = (aq+q\tau)t$, $h_{1i} = \left(2a_{2i}\varpi - 3a_{3i}\varpi^2\right)$ and $h_{2i} = (6a_{3i}\varpi)/q$. Equation (6) shows the coupling existing in (4) is removed. The purposes of introducing q are to limit h_{2i} and make sure $aq = 1$, and those will be described in Section III-C.

To estimate the parameters h_{1i} and h_{2i}, Fourier transform (FT) is performed along the t_{new} and τ, respectively, which is represented as

$$\mathrm{TFD}\left(f_{t_{new}}, f_\tau\right) = \mathrm{FT}_\tau[\mathrm{FT}_{t_{new}}[R_{s_m}(t_{new},\tau)]] \tag{7}$$

where f_τ and $f_{t_{new}}$ denote the frequency domain with respect to τ and t_{new}, respectively. $\mathrm{FT}_\tau[\cdot]$ and $\mathrm{FT}_{t_{new}}[\cdot]$ denote the FT operation along the τ and t_{new}, respectively. TFD is a 2D frequency domain about f_τ and $f_{t_{new}}$.

Substituting (6) into (7) yields

$$\begin{aligned} &\mathrm{TFD}\left(f_{t_{new}}, f_\tau\right) \\ &= \mathrm{FT}_\tau[\mathrm{FT}_{t_{new}}[\mathrm{IFT}_f[\mathrm{LSFT}_t\left(R_{s_m}(t,\tau)\right)]]] \\ &= \sum_{i=1}^{K} A_i^4 \exp\Big[\left(j2\pi h_{1i}a\right)\delta\left(f_\tau - h_{1i}\right) \\ &\qquad \times \delta\left(f_{t_{new}} - h_{2i}\right)\Big] + Q_{cross}\left(f_{t_{new}}, f_\tau\right) \end{aligned} \tag{8}$$

where $\delta(\cdot)$ denotes Dirac delta function and the $Q_{cross}(f_{t_{new}}, f_\tau)$ denotes the cross-term after FT operation. It is easily seen from (8) that each self-term can be accumulated as a sole peak at the point (h_{1i}, h_{2i}) where $1 \le i \le K$, and each peak denotes a QFM signal. Thus, there are K peaks in the TFD domain. By locating the peaks, the parameters h_{1i} and h_{2i} can be estimated. To obtain the estimation of a_{2i} and a_{3i}, we need to perform the transformation about the parameters which are expressed as

$$a_{2i} = \frac{h_{1i} + (qh_{2i}\varpi)/2}{2\varpi} \text{ and } a_{3i} = \frac{qh_{2i}}{6\varpi} \tag{9}$$

a_{1i} can be obtained by the dechirping and FFT operation which is presented in [19] and [20].

For $Q_{cross}\left(f_{t_{new}}, f_\tau\right)$, as long as the energy of the cross-term cannot be accumulated as the self-term, no peak appears in the TFD domain with related to the cross-term. However, for three special cases, the energy of the cross-term is accumulated as the self-term which will be verified in Appendix. In further study, we will focus on resolving this problem. In order to facilitate analysis, we assume that the energy of the cross-term cannot be accumulated.

It is worth noting that, according to (5), the $\mathrm{IFT}_f[\cdot]$ is the inverse transformation of $\mathrm{FT}_{t_{new}}[\cdot]$ where $\mathrm{FT}_{t_{new}}[\cdot]$ is the FT with respect to t_{new}. Thus, in (8), the $\mathrm{IFT}_f[\cdot]$ operation is avoided since we need to perform the $\mathrm{FT}_{t_{new}}[\cdot]$ operation, and the peak accumulation operation can be simplified as

$$\mathrm{TFD}\left(f_{t_{new}}, f_\tau\right) = \mathrm{FT}_\tau[\mathrm{LSFT}_t\left(R_{s_m}(t,\tau)\right)] \tag{10}$$

III. PROPOSED METHOD

In this Section, we describe the proposed method based on mono-component QFM signal and multi-component QFM signals, respectively. In the end, we discuss the parameter selection criterion of the DSTFD.

A. DSTFD BASED ON MONO-COMPONENT

According to the introduction of related works in Section II, this subsection describes the proposed method based on a discrete time mono-component QFM signal. For easier understanding, the implementation of the LSFT will be introduced firstly. Then, we will describe the processing procedure of proposed method.

1) THE IMPLEMENTATION OF LSFT

According to [29], we know that the CZT is able to provide arbitrary frequency resolution within the selected frequency band, and it can be implemented easily by the complex multiplications and FFT. The format of CZT is expressed by

$$\begin{aligned} \mathrm{CZT}[x(n)] &= \sum_{n=0}^{N-1} x(n) z_l^{-n} \\ &= \sum_{n=0}^{N-1} x(n) A^{-n} W^{nl}, \quad l = 0, 1, \cdots, L-1 \end{aligned} \tag{11}$$

where $x(n)$ is a discrete signal, L is an arbitrary integer which denotes frequency number. The factors A and W are expressed by $A = A_0 \exp(j\theta_0)$ and $W = W_0 \exp\left(-j\Delta_\phi\right)$, where A_0 is the vector radius length, W_0 is zooming factor, θ_0 is initial phase angle, and Δ_ϕ is angle increment.

Similar to the keystone transform, the LSFT can be implemented based on the CZT [26], [30]. According to the analysis in [30], to implement the LSFT, the factors in CZT should be set to $A_0 = 1$, $W_0 = 1$, $\theta_0 = 2\pi\frac{f_d}{f_s}b$, and $\Delta_\phi = 2\pi\frac{f_r}{Lf_s}b$, where $f_r = f_u - f_d$ called searching frequency band. Substituting these factors into (11), the LSFT is obtained

$$\mathbf{R_s^C} = \begin{bmatrix} R_s^C\left(-\frac{N}{2},-\frac{N}{2}\right) & R_s^C\left(-\frac{N}{2}+1,-\frac{N}{2}\right) & \cdots & R_s^C\left(\frac{N}{2}-1,-\frac{N}{2}\right) \\ R_s^C\left(-\frac{N}{2},-\frac{N}{2}+1\right) & R_s^C\left(-\frac{N}{2}+1,-\frac{N}{2}+1\right) & \cdots & R_s^C\left(\frac{N}{2}-1,-\frac{N}{2}+1\right) \\ \vdots & \vdots & \ddots & \vdots \\ R_s^C\left(-\frac{N}{2},\frac{N}{2}-1\right) & R_s^C\left(-\frac{N}{2}+1,\frac{N}{2}-1\right) & \cdots & R_s^C\left(\frac{N}{2}-1,\frac{N}{2}-1\right) \end{bmatrix} \tag{14}$$

which is represented by

$$\begin{aligned} \mathrm{LSFT}\left[x\left(n\right)\right] &= \sum_{n=0}^{N-1} x\left(n\right) z_l^{-n} \\ &= \sum_{n=0}^{N-1} x\left(n\right) \exp\left[-j2\pi\left(\frac{f_d}{f_s}bn + \frac{f_r}{Lf_s}bnl\right)\right] \end{aligned} \tag{12}$$

2) PROCESSING PROCEDURE OF DSTFD

For the mono-component QFM signal, the number of component is $K = 1$ in (1). In this part, the discrete mono-component QFM is simplified as

$$s\left(n\right) = A\exp\left[j2\pi\left(a_1nT_s + a_2(nT_s)^2 + a_3(nT_s)^3\right)\right], \quad (1 \le n \le N_w) \tag{13}$$

where T_s is the sampling interval. By performing the PISCF on $s\left(n\right)$, a two dimensional instantaneous self-correlation matrix is obtained which is written as (see (14), shown at the top of this page), where $N = (N_w - (\varpi + aq)/T_s)$ is the effective signal length. With the Claasen and Mecklenbrauker (CM) sampling scheme [31], the element in $\mathbf{R_s^C}$ is expressed as

$$R_s^C\left(n,m\right) = A^4\exp\left[j2\pi\left(h_1(a+2mT_s) + h_2(aq+2qmT_s)nT_s\right)\right] \tag{15}$$

where $h_1 = 2a_2\varpi - 3a_3\varpi^2$, $h_2 = 6a_3\varpi/q$, n is the sampling of time variable t with $-\frac{N}{2} \le n \le \frac{N}{2}-1$, and m is the sampling of lag variable τ with $-\frac{N}{2} \le m \le \frac{N}{2}-1$. For the matrix in (14), each row changes over time variable n and each column changes over the lag variable m. To estimate the parameters, the DS estimation strategy, which includes coarse estimation and fine estimation, is performed on $\mathbf{R_s^C}$.

a: COARSE ESTIMATION

According to (10), to accumulate peak, the LSFT and FT should be performed on $\mathbf{R_s^C}$ along the lag variable and time variable, respectively. For the coarse estimation, FT is implemented by FFT operation. Thus, the procedure is represented as

$$\mathrm{TDF}_1 = \mathrm{FFT}_{\mathrm{col}}\left[\mathrm{LSFT}_{\mathrm{row}}\left[\mathbf{R_s^C}\right]\right] \tag{16}$$

where $\mathrm{LSFT}_{\mathrm{row}}[\cdot]$ denotes the LSFT operation performing on the row, $\mathrm{FFT}_{\mathrm{col}}[\cdot]$ denotes the FFT operation performing on the columns, and TDF_1 is the 2D frequency domain which is obtained by performing the coarse estimation. By searching the peak on the TDF_1 domain, the rough estimations of h_1 and h_2 are obtained which are denoted by $\hat{h}_1$ and $\hat{h}_2$.

According to the analysis of LSFT in (5), for the coarse estimation operation, the searching range of LSFT is set to $f_d = -f_s/2$ and $f_u = f_s/2$ because the range of h_2 is unknown in advance.

Due to the CM sampling property, the sampling frequency of the time variable and the lag variable are equal to f_s and $f_s/2$, respectively. So the estimation precision of $\hat{h}_1$ and $\hat{h}_2$ are equal to $f_s/\left(2N\right)$ and f_s/L_1, respectively, where N is the frequency number for the FFT which is equal to effective signal length, and L_1 is the frequency number for the LSFT which is determined by the resolution requirement in practical application. In order to improve estimation precision, the fine estimation operation should be performed.

b: FINE ESTIMATION

Different from the coarse estimation, for the fine estimation, the searching frequency band is selected around $\hat{h}_1$ and $\hat{h}_2$. Moreover, CZT operation is performed instead of FFT operation to implement FT, because entire frequency band search is not needed. Thus, the fine estimation procedure is represented as

$$\mathrm{TDF}_2 = \mathrm{CZT}_{\mathrm{col}}\left[\mathrm{LSFT}_{\mathrm{row}}\left[\mathbf{R_s^C}\right]\right] \tag{17}$$

where $\mathrm{CZT}_{\mathrm{col}}[\cdot]$ denotes the CZT operation performing on the columns, and TDF_2 denotes the 2D frequency domain which is obtained by performing the fine estimation.

The searching frequency ranges of $\hat{h}_1$ and $\hat{h}_2$ are set to the estimation precision of the coarse estimation operation, which means that

$$f_{r,h_1} = f_s/\left(2N\right) \quad \text{and } f_{r,h_2} = f_s/L_1 \tag{18}$$

where f_{r,h_1} and f_{r,h_2} are the fine searching frequency ranges of $\hat{h}_1$ and $\hat{h}_2$, respectively. According to the searching frequency ranges, the factors θ_0 and Δ_ϕ of CZT are set as

$$\theta_0 = 2\pi\frac{\hat{h}_1 - f_{r,h_1}/2}{f_s} \quad \text{and} \quad \Delta\phi = 2\pi\frac{f_{r,h_1}}{f_sL_{CZT}} \tag{19}$$

where L_{CZT} is the frequency number.

Meanwhile, the factors f_d and f_u of LSFT are set as

$$f_d = \hat{h}_2 - f_{r,h_2}/2 \quad \text{and} \quad f_u = \hat{h}_2 + f_{r,h_2}/2 \tag{20}$$

and frequency number is set as L_2.

By locating the peak in the TDF_2 domain, the fine estimations of h_1 and h_2, which are denoted by $\hat{h}_1^{fine}$ and $\hat{h}_2^{fine}$, are obtained with the precision $\frac{f_s}{2NL_{CZT}}$ and $\frac{f_s}{L_1L_2}$, respectively. In this paper, we assume the estimation precision of each QFM parameter is the same, which means that $2NL_{CZT} = L_1L_2$. The value of L_1, L_2, and L_{CZT} are set in advance decided by the requirement of precision in practical application.

According to (9), The fine estimate of a_2 and a_3 are obtained by

$$\begin{aligned} \hat{a}_2^{fine} &= \frac{\hat{h}_1^{fine} + \left(q\hat{h}_2^{fine}\varpi\right)/2}{2\varpi} \\ \hat{a}_3^{fine} &= \frac{q\hat{h}_2^{fine}}{6\varpi} \end{aligned} \tag{21}$$

where $\hat{a}_2^{fine}$ and $\hat{a}_3^{fine}$ denote the fine estimations of a_2 and a_3. The fine estimate of a_1 represented as $\hat{a}_1^{fine}$ can be obtained by dechirping method [18], [19].

The proposed algorithm is summarized in Algorithm 1.

Algorithm 1

1: Input: The QFM signal $s(n)$, sampling frequency f_s, and frequency numbers L_1, L_2 and L_{CZT}.
2: Step 1: Perform PISCF given in (3) on $s(n)$ to obtain (14).
3: Step 2: Set $f_d = -f_s/2, f_u = f_s/2$ for the LSFT. Perform LSFT and FFT on (14) to obtain TDF_1 by (16).
4: Step 3: Search the peak in the TDF_1 domain to obtain the coarse estimated values $\hat{h}_1$ and $\hat{h}_2$.
5: Step 4: According to $\hat{h}_1$ and $\hat{h}_2$, calculate the factors for LSFT and CZT based on (18) to (20). Perform LSFT and CZT on (14) to obtain TDF_2 domain by (17).
6: Step 5: Search the peak in the TDF_2 domain to obtain the fine estimated values $\hat{h}_1^{fine}$ and $\hat{h}_2^{fine}$.
7: Step 6: Finally, the fine estimate of $\hat{a}_2^{fine}$ and $\hat{a}_3^{fine}$ are obtained by using (21), and the fine estimate $\hat{a}_1^{fine}$ are obtained by dechirping method.
8: Output: The final estimate of the QFM coefficients, $\hat{a}_1^{fine}$, $\hat{a}_2^{fine}$, and $\hat{a}_3^{fine}$.

B. DSTFD BASED ON MULTI-COMPONENT

For the multi-component QFM signals, the proposed method still works. The discrete form of (1) is expressed as

$$\begin{aligned} &s_m(n) \\ &= \sum_{i=1}^{K} A_i \exp[j2\pi(a_{1i}nT_s + a_{2i}(nT_s)^2 + a_{3i}(nT_s)^3)] \end{aligned} \tag{22}$$

According to the analysis of the peak accumulation technique presented in Section II-B, when we consider K QFM signals in the searching frequency range, K peaks will be accumulated in the TFD domain after performing the peak accumulation technique. Thus, by performing the coarse estimation operation on (22), there will be K peaks in the TFD_1 domain, and each peak denotes a QFM signal. According to locating the peaks in the TFD_1 domain, the coarse estimated parameters of the K QFM signals are obtained, which are represented by $\left\{\hat{h}_{1i}, \hat{h}_{2i}, i = 1, \cdots, K\right\}$. For the fine estimate operation, according to the coarse estimation parameters, we set different factors for CZT and LSFT. Such as, for the estimated parameters of the ith peak, the factors of LSFT should be set as

$$f_{di} = \hat{h}_{2i} - f_{r,h_2}/2 \quad \text{and} \quad f_{ui} = \hat{h}_{2i} + f_{r,h_2}/2 \tag{23}$$

and the factors ofc CZT should be set as

$$\theta_{0i} = 2\pi\frac{\hat{h}_{1i} - f_{r,h_1}/2}{f_s} \quad \text{and} \quad \Delta\phi_i = 2\pi\frac{f_{r,h_1}}{f_s L_{CZT}} \tag{24}$$

where f_{r,h_1} and f_{r,h_2} are the fine search frequency ranges which are the same as those for the mono-component case. With the above factors, the fine estimated values $\hat{h}_{1i}^{fine}$ and $\hat{h}_{2i}^{fine}$ are obtained by using fine estimation operation. According to (9), the fine estimations of a_{2i} and a_{3i} are expressed as

$$\hat{a}_{2i}^{fine} = \frac{\hat{h}_{1i}^{fine} + \left(\hat{h}_{2i}^{fine}\varpi\right)/2}{2\varpi} \quad \text{and} \quad \hat{a}_{3i}^{fine} = \frac{\hat{h}_{2i}^{fine}}{6\varpi} \tag{25}$$

The fine estimation of a_{1i} is estimated by dechirping operation [18], [19].

C. PARAMETER SELECTION

In this part, the selection criteria of the parameters including ϖ, a, and q are discussed. According to the analyses and simulations in [27] and [28], ϖ can not only reduce the number of self-correlations but also complete the order reduction which benefits the anti-noise performance and the energy accumulation. The optimal ϖ is equal to $N_wT_s/3$ which has been proved in [16] based on an alternative optimality criterion (the resolution capability).

The delay a is corresponding to the keystone transform [26]. Based on the analysis in (6), $t_{new} = (aq + q\tau)t$. Lv *et al.* [30] propose a phase lines analysis method to analyze the choice of aq. In order to guarantee precision and improve anti-noise ability, the optimal value of aq is equal to one, because no interpolation is required along the axis t_{new} and the interpolation on both sides of the axis is symmetrical. Define the discrete parameter pair (a, q) as (N_rT_s, q). Assume the given number of time sampling points of the PISCF is N, then

$$N_r = N_w - N \quad \text{and} \quad q = \frac{1}{(N_w - N)T_s} \tag{26}$$

It is easily seen that (26) makes sure $aq = 1$. In addition, the previously processed data can be used as the redundancy information to perform the proposed method.

TABLE 1. The parameters of two component QFM signals.

QFM	A	a_1/Hz	a_2/Hz	a_3/Hz
Component 1	1	10×10^6	16×10^{12}	4×10^{18}
Component 2	1	20×10^6	9.5×10^{12}	2×10^{18}

IV. PERFORMANCE ANALYSIS

In order to verify the effectiveness of the proposed method, anti-noise performance and computational cost will be analyzed for the proposed method. According to the analysis in Introduction, the HAF-ICPF [19] and the algorithm presented in [25] are selected as the comparative method. The parameters of the QFM signals are given in Table 1.

A. ANTI-NOISE PERFORMANCE

In this subsection, the anti-noise performance will be analyzed for the DSTFD, the HAF-ICPF, and the algorithm presented in [25]. For statistical study the estimation performance of the proposed method, it is assessed by means of the normalized mean square error (NMSE) [32] expressed as

$$\mathrm{NMSE} = 10\log\left(\sum_{l=1}^{N_{\mathrm{trails}}}\left(\hat{a}_l - a_l\right)^2 / \sum_{l=1}^{N_{\mathrm{trails}}} a_l^2\right) \tag{27}$$

where N_{trails} denotes the number of trails (here $N_{\mathrm{trails}} = 300$) and $\hat{a}_l$ is the estimation of the a in the lth trial. The evaluation is based on noisy mono-component QFM signal and noisy multi-component QFM signals.

1) MONO-COMPONENT QFM SIGNAL CASE

The signal used in this simulation is the first component shown in Table 1. The sampling frequency is 128 MHz. The effective signal length is 512. The signal is corrupted by an additive Gaussian noise with signal-to-noise ratio (SNR) $\in [-8 : 0]$ dB, which is changed in increments of 1 dB. The simulation results are shown in Fig. 1.

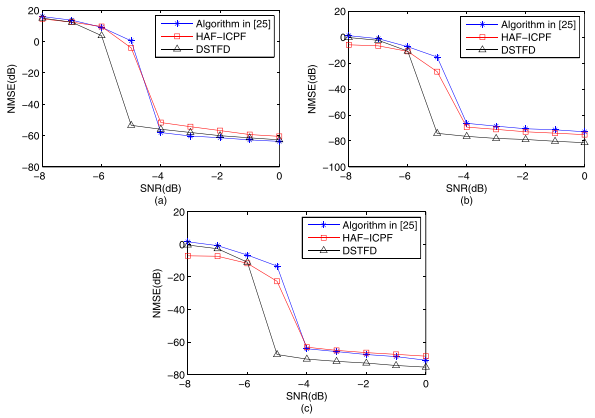

FIGURE 1. NMSEs for the DSTFD, the HAF-ICPF, and the algorithm presented in [25]. (a) NMSEs of a_1. (b) NMSEs of a_2. (c) NMSEs of a_3.

Fig. 1 shows the NMSE results of the DSTFD, the HAF-ICPF, and the algorithm presented in [25]. It is easily seen that both the SNR thresholds of the HAF-ICPF and the algorithm presented in [25] are -4 dB. The SNR threshold of the DSTFD is -5 dB. Therefore, the anti-noise performance of DSTFD is better than that of other two methods. That is because, compared with other methods, DSTFD introduces the constant delay which can increase energy accumulation and improve anti-noise ability. Moreover, Fig. 1 shows that the estimation accuracy of a_1 of DSTFD is close to algorithm presented in [25], and it is better than that of the HAF-ICPF. Meanwhile, the accuracy of a_2 and a_3 of DSTFD is better than that of the other two methods. According to the analysis in Section III-C, the delay a helps to avoid the non-uniformly spaced lag-time axis which is beneficial to improve accuracy. Therefore, it can be concluded that the anti-noise ability of the proposed method is improved, and the estimation accuracy is still satisfactory.

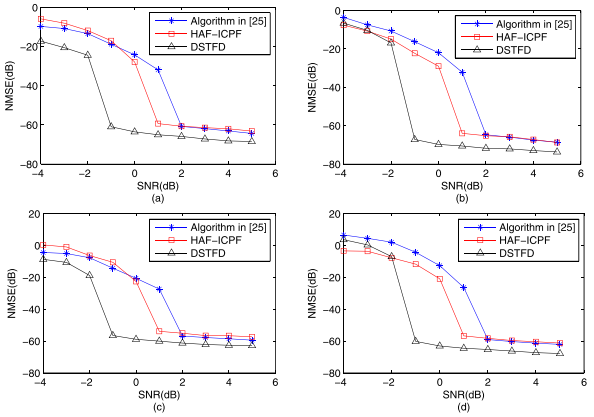

FIGURE 2. NMSEs for a_3 and a_2 of the two component QFM signals. (a) NMSEs for a_2 of the first component QFM. (b) NMSEs for a_3 of the first component QFM. (c) NMSEs for a_2 of the second component QFM. (b) NMSEs for a_3 of the second component QFM.

2) MULTI-COMPONENT QFM SIGNALS CASE

For multi-component QFM case, we consider two component QFM signals, and the parameters are given in Table 1. The sampling frequency is 128 MHz, and the effective signal lengths are equal to 512. The signals are corrupted by an additive Gaussian noise with SNR $\in [-4 : 5]$ dB changed in increments of 1 dB, and they are also assessed by NMSE. In this simulation, only the two highest order coefficients are given due to brevity. Fig. 2 depicts the NMSEs for a_3 and a_2 of two component QFM signals given in Table 1, where Fig. 2(a) and Fig. 2(b) are corresponding to the first component and Fig. 2(c) and Fig. 2(d) are corresponding to the second component. SNR thresholds of the algorithm in [25], the HAF-ICPF, and the DSTFD are 2 dB, 1dB, and -1 dB, respectively. Compared to the algorithm in [25], the DSTFD can achieve better anti-noise performance because constant delay is introduced in the DSTFD which contributes to improve anti-noise ability and energy accumulation. For the HAF-ICPF, since the CLEAN operation [19] is used to estimate the multi-component, the anti-noise ability decreases. Therefore, the anti-noise ability of the DSTFD is better than

that of the other two methods for multi-component. Meanwhile, Fig. 2 shows that the estimation accuracy of DSTFD is also satisfactory.

B. COMPUTATIONAL COST

According to the analysis in Section III-A, by using the DSTFD method, the parameters estimation precision is $f_s/(2NL_{CZT})$. In this part, the computational costs of HAF-ICPF, the algorithm presented in [25], and DSTFD are analyzed based on the same precision.

For the HAF-ICPF, the main implementation procedures are HAF and ICPF, and the computational costs of them are $O(N)$ and $O((NL_{CZT})^3)$, respectively. Therefore, the computational cost of HAF-ICPF is $O((NL_{CZT})^3)$ [19]. For the algorithm presented in [25], its main implementation procedures include a parametric self-correlation function, the GSCFT, and the FFT operation. The computational costs of them are $O\left(N^2\right)$, $O\left((NL_{CZT})^2\log_2(NL_{CZT})\right)$, and $O\left((NL_{CZT})^2\log_2(NL_{CZT})\right)$, respectively. Thus, the overall computational cost of the algorithm presented in [25] is $O\left((NL_{CZT})^2\log_2(NL_{CZT})\right)$ [25]. For the DSTFD method, its main implementation procedures include the PISCF, the LSFT, the FFT, and the CZT. The computational costs of them are $O\left(N^2\right)$, $O\left(N^2\log_2 N\right)$, $O\left(N^2\log_2 N\right)$, and $O\left((N+L_{CZT})^2\log_2(N+L_{CZT})\right)$ [29], respectively. Thus, the overall computational cost of DSTFD is $O\left((N+L_{CZT})^2\log_2(N+L_{CZT})\right)$. Table 2 gives computational costs of these three estimation algorithms.

TABLE 2. Computational costs.

The algorithm presented in [26]	$O((NL_{CZT})^2\log_2(NL_{CZT}))$
HAF-ICPF	$O((NL_{CZT})^3)$
DSTFD	$O((N+L_{CZT})^2\log_2(N+L_{CZT}))$

It is easily seen from Table 2 that the computational cost of DSTFD is lower than that of the other two methods. According to the analysis in Section III-A, when the signal effective length N is not changed, L_{CZT} should be large to obtain high estimation precision. For the DSTFD, the computational cost is almost unchanged with the increase of L_{CZT}. However, for the algorithm presented in [25] and the HAF-ICPF, the computational costs are sensitive to L_{CZT}.

To illustrate the superiority of the proposed algorithm, the computational cost of different precision is shown by using the average simulation time, which is depicted in Fig. 3. The simulation condition is the same with the mono-component QFM signal simulation with SNR $= 0$ dB. The vertical axis shows the average simulation time, and the horizontal axis shows the estimation precision. The simulations are completed on a computer with an Intel Core I7-8700K (3.70GHz), 32 GB memory, and 64 bit operating system. The MATLAB version is R2018a. It is easily seen from Fig. 3, with the precision becoming higher, simulation times of the algorithm presented in [25] and the HAF-ICPF increase quickly. For the DSTFD, the simulation time is

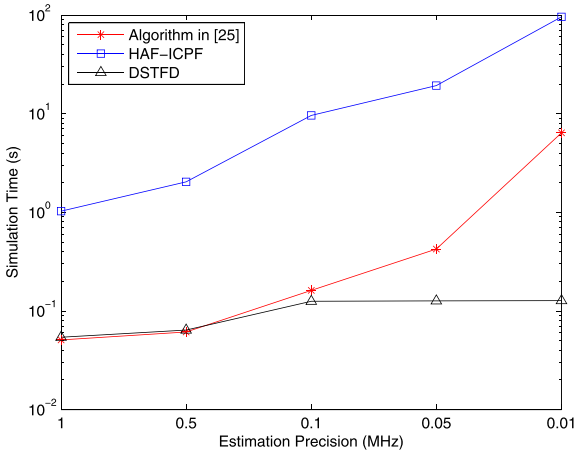

FIGURE 3. Simulation time.

almost unchanged with the precision increasing, and it is less than that of the other two methods. It is worth noting that when precision conditions are 1 MHz and 0.5 MHz, the DSTFD costs less simulation time than other precision conditions, because the DSTFD only needs to perform coarse estimation operation when the precision requirement is low.

V. CONCLUSION

In this paper, a novel method called DSTFD is developed to estimate both mono-component QFM signal and multi-component QFM signals. In the DSTFD, by using the PISCF and the idea of keystone transform operation on the QFM signals, the signal order is reduced and the coupling is removed. The computational cost is effectively reduced by using double scale estimation strategy, especially for obtaining high precision estimation. With numerical simulations about anti-noise performance and computational cost, we can see that the proposed method can obtain better anti-noise ability and less amount of calculation compared with other methods. Although the DSTFD can acquire higher anti-noise performance than other correlation methods, the performance is still not satisfactory because of the limitation of self-correlation function. In the near further, we mainly focus on following research work for the DSTFD: (1) developing of the high order version of the DSTFD for the general polynomial phase signals; (2) resolving the cross-term problem when it accumulates as the self-term; (3) improving the anti-noise performance of DSTFD.

APPENDIX

In this Appendix, we discuss the conditions when the cross-term is accumulated as the self-term in (8). To formulate the cross-term problem arising from multi-component QFM signals, we consider two QFM signals which is expressed as

$$s_m(t) = A_1 \exp\left(j2\pi\left(a_{11}t + a_{21}t^2 + a_{31}t^3\right)\right) + A_2 \exp\left(j2\pi\left(a_{12}t + a_{22}t^2 + a_{32}t^3\right)\right) \quad (28)$$

$$
\begin{aligned}
&Q_{cross,1}\\
&= \mathrm{FT}_\tau\{\mathrm{LSFT}_t\{A_1^2A_2^2\exp\{j2\pi[(\varphi_1+M_4)(a+\tau)+2(\varphi_2+3a_{32}\varpi)(a+\tau)t)]\}\exp\{j2\pi[2\varphi_3(\frac{a+\tau}{2})^3+3\varphi_3(a+\tau)t^2]\}\\
&\quad + A_1^2A_2^2\exp\{j2\pi[(M_3-\varphi_1)(a+\tau)+2(3a_{31}\varpi-\varphi_2)(a+\tau)t)]\}\exp\{-j2\pi[2\varphi_3(\frac{a+\tau}{2})^3+3\varphi_3(a+\tau)t^2]\}\}\}
\end{aligned}
\tag{30}
$$

$$
\begin{aligned}
&Q_{cross,2}\\
&= \mathrm{FT}_\tau\{\mathrm{LSFT}_t\{A_1^2A_2^2\exp\{j2\pi[(M_3+M_4)\frac{a+\tau}{2}+3(a_{31}\varpi+a_{32}\varpi)(a+\tau)t]\}\\
&\quad \times\cos\{2\pi[(M_1-M_2)+2(\varphi_2\varpi-\varphi_3\varpi^2)t+3\varphi_3\varpi t^2+3\varphi_3\varpi(\frac{a+\tau}{2})^2]\}\}\}
\end{aligned}
\tag{31}
$$

$$
\begin{aligned}
&Q_{cross,3}\\
&= \mathrm{FT}_\tau\{\mathrm{LSFT}_t\{\{A_1^3A_2\exp\{j2\pi[(\varphi_1+M_3+M_4)\frac{a+\tau}{2}+(\varphi_2+3a_{31}\varpi+3a_{32}\varpi)(a+\tau)t]\}\\
&\quad \times\cos\{2\pi[(M_2-M_1)+(\varphi_1-2\varphi_2\varpi+3\varphi_3\varpi^2)t+(\varphi_2-3\varphi_3\varpi)t^2+(\varphi_2-3\varphi_3\varpi)(\frac{a+\tau}{2})^2]\\
&\quad + A_1A_2^3\exp\{j2\pi[(\varphi_1+2M_4)\frac{a+\tau}{2}+(\varphi_2+6a_{32}\varpi)(a+\tau)t]\}\cos\{2\pi[\varphi_1t+\varphi_2t^2+\varphi_2(\frac{a+\tau}{2})^2]\}\}\\
&\quad \times\exp\{j2\pi\varphi_3[\frac{(a+\tau)^3}{4}+3(a+\tau)t^2]\}\}\}
\end{aligned}
\tag{32}
$$

$$
\begin{aligned}
&Q_{cross,4}\\
&= \mathrm{FT}_\tau\{\mathrm{LSFT}_t\{\{A_1A_2^3\exp\{j2\pi[(M_3+M_4-\varphi_1)\frac{a+\tau}{2}+(3a_{31}\varpi+3a_{32}\varpi-\varphi_2)(a+\tau)t]\}\\
&\quad \times\cos\{2\pi[(M_1-M_2)+(2\varphi_2\varpi-3\varphi_3\varpi^2-\varphi_1)t+(3\varphi_3\varpi-\varphi_2)t^2+(3\varphi_3\varpi-\varphi_2)(\frac{a+\tau}{2})^2]\\
&\quad + A_1^3A_2\exp\{j2\pi[(2M_3-\varphi_1)\frac{a+\tau}{2}+(6a_{31}\varpi-\varphi_2)(a+\tau)t]\}\cos\{2\pi[\varphi_1t+\varphi_2t^2+\varphi_2(\frac{a+\tau}{2})^2]\}\}\\
&\quad \times\exp\{-j2\pi\varphi_3[\frac{(a+\tau)^3}{4}+3(a+\tau)t^2]\}\}\}
\end{aligned}
\tag{33}
$$

$$
\begin{aligned}
&Q_{cross,5}\\
&= \mathrm{FT}_\tau\{\mathrm{LSFT}_t\{A_1^2A_2^2\exp\{j2\pi[(M_3+M_4)\frac{a+\tau}{2}+(3a_{31}\varpi+3a_{32}\varpi)(a+\tau)t]\}\\
&\quad \times\cos\{2\pi[(M_2-M_1)+(2\varphi_1-2\varphi_2\varpi+3\varphi_3\varpi^2)t+(2\varphi_2-3\varphi_3\varpi)(t^2+(\frac{a+\tau}{2})^2)+6\varphi_3t(\frac{a+\tau}{2})^2+2\varphi_3t^3]\}\}\}
\end{aligned}
\tag{34}
$$

With careful analyses of the characteristics of the cross-term, Q_{cross} can be divided into five parts and represented as

$$Q_{cross} = Q_{cross,1} + Q_{cross,2} + Q_{cross,3} + Q_{cross,4} + Q_{cross,5} \tag{29}$$

Let

$$M_1 = \left(a_{11}\varpi - a_{21}\varpi^2 + a_{31}\varpi^3\right),$$
$$M_2 = \left(a_{12}\varpi - a_{22}\varpi^2 + a_{32}\varpi^3\right),$$
$$M_3 = \left(2a_{21}\varpi - 3a_{31}\varpi^2\right), \quad M_4 = \left(2a_{22}\varpi - 3a_{32}\varpi^2\right),$$
$$\varphi_1 = (a_{11} - a_{12}), \quad \varphi_2 = (a_{21} - a_{22}),$$

and

$$\varphi_3 = (a_{31} - a_{32}).$$

$Q_{cross,1}$, $Q_{cross,2}$, $Q_{cross,3}$, $Q_{cross,4}$, and $Q_{cross,5}$ can be presented as (30)-(32), as shown at the top of this page, (33) and (34), as shown at the top of this page.

Based on characteristics of $Q_{cross,1}$, $Q_{cross,2}$, $Q_{cross,3}$, $Q_{cross,4}$, and $Q_{cross,5}$, we obtain that, (1) when $a_{31} = a_{32}$, $Q_{cross,1}$ can accumulate as the self-term; (2) when $a_{21} = a_{22}$ and $a_{31} = a_{32}$, $Q_{cross,2}$ can accumulate as the self-term; (3) when $a_{11} = a_{12}$, $a_{21} = a_{22}$, and $a_{31} = a_{32}$, $Q_{cross,3}$, $Q_{cross,4}$, and $Q_{cross,5}$ can accumulate as the self-term. It concluded that when the cross-term satisfies any of the above conditions, the cross-term can accumulate as the self-term. In further study and research, we will focus on this problem.

REFERENCES

[1] P. O'Shea, "A fast algorithm for estimating the parameters of a quadratic FM signal," *IEEE Trans. Signal Process.*, vol. 52, no. 2, pp. 385–393, Feb. 2004.

[2] J. Zheng, H. Liu, and Z. Liu, "Parameterized two-dimensional representation for multicomponent cubic phase signals and its application in ISAR imaging of fluctuating ship," *Digit. Signal Process.*, vol. 78, pp. 218–231, Jul. 2018.

[3] P. Ye *et al.*, "Parameter estimation of QFM signal based on MPKF," *Digit. Signal Process.*, vol. 76, pp. 1–13, May 2018.

[4] J. Zheng, H. Liu, Z. Liu, and Q. H. Liu, "ISAR imaging of ship targets based on an integrated cubic phase bilinear autocorrelation function," *Sensors*, vol. 17, no. 3, p. 498, Mar. 2017.
[5] T. J. Abatzoglou, "Fast maximum likelihood joint estimation of frequency and frequency rate," *IEEE Trans. Aerosp. Electron. Syst.*, vol. AES-22, no. 6, pp. 708–715, Nov. 1986.
[6] S. Golden and B. Friedlander, "Maximum likelihood estimation, analysis, and applications of exponential polynomial signals," *IEEE Trans. Signal Process.*, vol. 47, no. 6, pp. 1493–1501, Jun. 1999.
[7] L. Wu, X. Wei, D. Yang, H. Wang, and X. Li, "ISAR imaging of targets with complex motion based on discrete chirp Fourier transform for cubic chirps," *IEEE Trans. Geosci. Remote Sens.*, vol. 50, no. 10, pp. 4201–4212, Oct. 2012.
[8] Y. Wang and Y. Jiang, "ISAR imaging of maneuvering target based on the L-class of fourth-order complex-lag PWVD," *IEEE Trans. Geosci. Remote Sens.*, vol. 48, no. 3, pp. 1518–1527, Mar. 2010.
[9] Y. Wang, J. Kang, and Y. Jiang, "ISAR imaging of maneuvering target based on the local polynomial Wigner distribution and integrated high-order ambiguity function for cubic phase signal model," *IEEE J. Sel. Topics Appl. Earth Observ. Remote Sens.*, vol. 7, no. 7, pp. 2971–2991, Jul. 2014.
[10] Y. Wang, B. Zhao, and J. Kang, "Asymptotic statistical performance of local polynomial Wigner distribution for the parameters estimation of cubic-phase signal with application in ISAR imaging of ship target," *IEEE J. Sel. Topics Appl. Earth Observ. Remote Sens.*, vol. 8, no. 3, pp. 1087–1098, Mar. 2015.
[11] I. Djurovic and L. J. Stankovic, "Quasi-maximum-likelihood estimator of polynomial phase signals," *IET Signal Process.*, vol. 13, no. 4, pp. 347–359, Jun. 2014.
[12] H. Liu, D. Li, Y. Zhou, and T.-K. Truong, "Simultaneous radio frequency and wideband interference suppression in SAR signals via sparsity exploitation in time–frequency domain," *IEEE Trans. Geosci. Remote Sens.*, vol. 56, no. 10, pp. 5780–5793, Oct. 2018.
[13] S. Peleg and B. Porat, "Linear FM signal parameter estimation from discrete-time observations," *IEEE Trans. Aerosp. Electron. Syst.*, vol. 27, no. 4, pp. 607–616, Jul. 1991.
[14] P. O'Shea, "A new technique for instantaneous frequency rate estimation," *IEEE Signal Process. Lett.*, vol. 9, no. 8, pp. 251–252, Aug. 2002.
[15] S. Barbarossa and V. Petrone, "Analysis of polynomial-phase signals by the integrated generalized ambiguity function," *IEEE Trans. Signal Process.*, vol. 45, no. 2, pp. 316–327, Feb. 1997.
[16] S. Barbarossa, A. Scaglione, and G. B. Giannakis, "Product high-order ambiguity function for multicomponent polynomial-phase signal modeling," *IEEE Trans. Signal Process.*, vol. 46, no. 3, pp. 691–708, Mar. 1998.
[17] Y. Wang and Y. Jiang, "Inverse synthetic aperture radar imaging of maneuvering target based on the product generalized cubic phase function," *IEEE Geosci. Remote Sens. Lett.*, vol. 8, no. 5, pp. 958–962, Sep. 2011.
[18] Y. Wang and Y. Jiang, "ISAR imaging of a ship target using product high-order matched-phase transform," *IEEE Geosci. Remote Sens. Lett.*, vol. 6, no. 4, pp. 658–661, Oct. 2009.
[19] Y. Wang, "Inverse synthetic aperture radar imaging of manoeuvring target based on range-instantaneous- doppler and range-instantaneous-chirp-rate algorithms," *IET Radar, Sonar Navigat.*, vol. 6, no. 9, pp. 921–928, Dec. 2012.
[20] J. Zheng, T. Su, L. Zhang, W. Zhu, and Q. H. Liu, "ISAR imaging of targets with complex motion based on the chirp rate–quadratic chirp rate distribution," *IEEE Trans. Geosci. Remote Sens.*, vol. 52, no. 11, pp. 7276–7289, Nov. 2014.
[21] Y. Li, "Inverse synthetic aperture radar imaging of targets with complex motions based on modified chirp rate-quadratic chirp rate distribution for cubic phase signal," *J. Appl. Remote Sens.*, vol. 9, no. 1, Jan. 2016.
[22] Z. Qu, F. Qu, C. Hou, and F. Jing, "Quadratic frequency modulation signals parameter estimation based on two-dimensional product modified parameterized chirp rate-quadratic chirp rate distribution," *Sensors*, vol. 18, no. 5, p. 1624, May 2018.
[23] X. Bai, R. Tao, Z. Wang, and Y. Wang, "ISAR imaging of a ship target based on parameter estimation of multicomponent quadratic frequency-modulated signals," *IEEE Trans. Geosci. Remote Sens.*, vol. 52, no. 2, pp. 1418–1429, Feb. 2014.
[24] W. Cui, S. Wu, J. Tian, D. Liu, and S. Wu, "Parameter estimation for maneuvering targets with complex motion via scaled double-autocorrelation transform," *Digit. Signal Process.*, vol. 59, pp. 31–48, Dec. 2016.
[25] J. Zheng, H. Liu, G. Liao, T. Su, Z. Liu, and Q. H. Liu, "ISAR imaging of targets with complex motions based on a noise-resistant parameter estimation algorithm without nonuniform axis," *IEEE Sensors J.*, vol. 16, no. 8, pp. 2509–2518, Apr. 2016.
[26] X. Lv, G. Bi, C. Wan, and M. Xing, "Lv's Distribution: Principle, implementation, properties, and performance," *IEEE Trans. Signal Process.*, vol. 59, no. 8, pp. 3576–3591, Aug. 2011.
[27] Y. Li, T. Su, J. Zheng, and X. He, "ISAR imaging of targets with complex motions based on modified Lv's distribution for cubic phase signal," *IEEE J. Sel. Topics Appl. Earth Observ. Remote Sens.*, vol. 8, no. 10, pp. 4775–4784, Oct. 2015.
[28] F. Jing, S. Jiao, C. Hou, W. Si, and Y. Wang, "Analysis of maneuvering targets with complex motions by two-dimensional product modified Lv's distribution for quadratic frequency modulation signals," *Sensors*, vol. 17, no. 6, p. 1460, Jun. 2017.
[29] L. Rabiner, R. Schafer, and C. Rader, "The chirp z-transform algorithm," *IEEE Trans. Audio Electroacoustics*, vol. 17, no. 2, pp. 86–92, Jun. 1969.
[30] X. Lv, M. Xing, C. Wan, and S. Zhang, "ISAR imaging of maneuvering targets based on the range centroid Doppler technique," *IEEE Trans. Image Process.*, vol. 19, no. 1, pp. 141–153, Jan. 2010.
[31] T. A. C. M. Claasen and W. F. G. Mecklenbrauker, "The Wigner distribution—A tool for time-frequency signal analysis. II. Discrete time signals," *Philips J. Res.*, vol. 35, pp. 276–300, 1980.
[32] T. Dong, Y. Lei, and J. Yang, "An algorithm for underdetermined mixing matrix estimation," *Neurocomputing*, vol. 104, pp. 26–34, Mar. 2013.

FULONG JING was born in 1990. He received the B.S. degree in electronics and information engineering from Harbin Engineering University, in 2013, where he is currently pursuing the Ph.D. degree. His research interests include radar signal processing and array signal processing.

CHUNJIE ZHANG was born in Harbin in 1975. She received the B.E. and Ph.D. degrees from Harbin Engineering University, in 2004 and 2006, respectively. From 2015 to 2016, she was a Visiting Scholar with Wright State University. She is currently an Associate Professor with the College of Information and Communication Engineering, Harbin Engineering University. Her main research interests include wideband channelized receiver, pulse compression signal processing, and microwave spectrum analysis based on the photonic signal processing.

WEIJIAN SI was born in Beijing. He received the B.E. degree from Beihang University, in 1994, and the Ph.D. degree from Harbin Engineering University, in 2004. From 1995 to 1999, he was with the 35th Institute of China Aerospace Science and Industry Corporation and was engaged in scientific research on radar signal processing. He is currently a Professor and a Ph.D. Supervisor with the College of Information and Communication Engineering, Harbin Engineering University, Heilongjiang, China. His main research interests include radar signal detection, processing and identification, high precision passive direction finding, and spatial spectrum estimation.

YU WANG was born in 1990. She received the B.S. degree in electronics and information engineering from Harbin Engineering University, in 2013, where she is currently pursuing the Ph.D. degree. Her research interests include blind souse separation, frequency hopping signal processing, and sparse Bayesian learning.

SHUHONG JIAO was born in 1966. She is currently a Professor and a Ph.D. Supervisor with the College of Information and Communication Engineering, Harbin Engineering University, Heilongjiang, China. She is a member of the Chinese Image Graphics Association and the Heilongjiang Institute of Biomedical Engineering. Her main research interests include image processing, machine vision, and radar signal processing.